*Journal of Statistical Physics, Vol. 81, Nos. 3/4, 1995*

# Scaling, Propagation, and Kinetic Roughening of Flame Fronts in Random Media

**Nikolas Provatas,[1] Tapio Ala-Nissila,[1,2,3] Martin Grant,[1] K. R. Elder,[1] and Luc Piché[1,4]**

*Received January 24, 1995; final May 11, 1995*

We introduce a model of two coupled reaction–diffusion equations to describe the dynamics and propagation of flame fronts in random media. The model incorporates heat diffusion, its dissipation, and its production through coupling to the background reactant density. We first show analytically and numerically that there is a finite critical value of the background density below which the front associated with the temperature field stops propagating. The critical exponents associated with this transition are shown to be consistent with mean-field theory of percolation. Second, we study the kinetic roughening associated with a moving planar flame front above the critical density. By numerically calculating the time-dependent width and equal-time height correlation function of the front, we demonstrate that the roughening process belongs to the universality class of the Kardar–Parisi–Zhang interface equation. Finally, we show how this interface equation can be analytically derived from our model in the limit of almost uniform background density.

**KEY WORDS:** Flame fronts; kinetic roughening; KPZ equation; percolation transition; reaction–diffusion systems.

## 1. INTRODUCTION

Systems out of equilibrium undergoing a transition from a metastable or unstable state to a stable phase often develop a front or interface between

[1] Physics Department, Rutherford Building, McGill University, Montréal, Québec, Canada H3A 2T8.

[2] Research Institute for Theoretical Physics, University of Helsinki, FIN-00014 University of Helsinki, Finland, and Department of Physics, Tampere University of Technology, FIN-33101 Tampere, Finland.

[3] Department of Physics, Brown University, Providence, Rhode Island 02912.

[4] Industrial Materials Institute, National Research Council of Canada, Boucherville, Québec, Canada, J4B 6Y4.



0022-4715/95/1100-0737$07.50/0 

the two phases. This front can play a crucial role in determining the dynamics of the transition. There are many systems, arising in various areas of science, that are characterized by the emergence of such a front, such as domain walls in the kinetics of phase transitions[1] and systems undergoing chemical reactions.[2] This paper will study a common but a particularly spectacular example involving the emergence of a reaction front in combustion, where a flame front forms and can propagate in a medium of randomly distributed reactants.[3]

A popular description of moving fronts involves using discrete cellular automaton models or coupled map lattices. Examples include wave propagation in excitable media[4] and front propagation for the description of the spread of epidemics.[5] Despite their superficial simplicity, such lattice models can exhibit complex behavior. A good example is a recently studied coupled map lattice with oscillatory local elements, which has been shown to exhibit a wide variety of complex dynamics.[6] In particular, the moving front associated with the model was shown to exhibit kinetic roughening analogous to pure interface growth equations.[1]

On a more microscopic level, an approach based on continuum reaction–diffusion equations has been extensively used in the chemical literature.[2] Often such nonlinear partial differential equations can be studied from the nonlinear dynamics point of view to reproduce many experimentally observed phenomena, such as spiral waves and chemical oscillations.[7] In the area of combustion of laminar flames in continuous media, the work of Sivashinsky[8,9] demonstrates how such equations can be qualitatively mapped into nonlinear interface equations describing the propagation of flame fronts. Despite much work, however, many properties of such equations and their connection to interface growth equations remain poorly understood, as does their precise quantitative relationship to combustion.

Lattice models similar to those studied studied in the papers above have also been used to study "forest fire" models.[10–12] However, no particular attention has been focused on the properties of the reaction front. Indeed, the majority of automaton models of forest fires do not include flame fronts.

In this work our aim is to study systematically the dynamics of slow combustion by deriving—from the microscopic physical principles behind combustion—a phase-field reaction–diffusion model.[5] Some of these results have been given in a short paper.[14] This model includes, in a realistic manner, the diffusion of heat, as well as the dissipation and production of heat through an activated chemical reaction occuring within the background

[5] By *slow* combustion, we mean that shock waves play no role in the process.[13]

density field. While our model also incorporates the effect of convection, this paper will focus on combustion in the absence of it. The model is investigated both analytically and numerically, using methods developed in the study of phase transitions to unravel the asymptotic behavior of a self-sustanining combustion front growing within a medium of *randomly distributed* reactants. We examine the dynamics of the front from the percolation point of view, as well as that of kinetic roughening of interfaces. Both the formation of the front, as well as its universal dependence on length and time are examined. Most importantly, we show that the combustion front exists only when the reactant concentration is greater than a critical value $c^* > 0$ in two dimensions. Moreover, we estimate the scaling exponents associated with the disappearance of the propagating front, and show that the behavior near $c^*$ is consistent with that of a mean-field percolation transition. Above the critical concentration, we find that the combustion front exhibits kinetic roughening. We then show both analytically and numerically that the kinetic roughening is described by the nonlinear Kardar–Parisi–Zhang (KPZ) interface equation.[15]

In order to be able to refer to a specific example when dealing with flame propagation, we will motivate it below in the context of forest fires. The physics associated with forest fires has recently received increasing attention[10–12] due to the potential relationship to the concept of self-organized criticality, introduced by Bak[16] and collaborators. In most cases studied, forest fires have been modeled through the use of cellular automaton models on a lattice.[11,12] In these works a collection of trees which can burn and subsequently reappear is considered. In contrast, in this work reactant cannot spontaneously reappear and the reaction front is defined only as long as there is a reactant present. Most importantly, our model is constructed from the fundamental physics of reaction–diffusion systems, rather than by introducing lattice rules. Thus, it realistically captures the various physical phenomena associated with reaction fronts.

This paper is organized as follows. In Section 2 we derive our phase field model. In Section 3 we consider the propagation of the flame front, and argue that there exists a percolation transition in the model, corresponding to a critical value of the density. The nature of this transition is examined first in the mean-field limit, and then numerically. In Section 4 the kinetic roughening of a planar reaction front is studied. We first study it numerically, then we derive an approximate equation of motion for the interface which is shown to be identical to the KPZ equation in the long-wavelength limit. Finally, Section 5 concludes and summarizes the results of this paper.

## 2. THE MODEL

Our model describes flame propagation through the dynamics of two fields inherent in the combustion process: the thermal field and a field describing the concentration of reactants. Specifically, it consists of two coupled reaction–diffusion equations, one for evolution of the thermal field $T(\mathbf{x}, t)$ at position $\mathbf{x}$ and time $t$, and the other describing the evolution of the reactant concentration $C(\mathbf{x}, t)$. This model realistically incorporates the interplay between thermal diffusion and local concentration fields. Within our model, variations in $T(\mathbf{x}, t)$ are due to three effects: (i) thermal diffusion through the medium in which the flames propagate; (ii) Newtonian cooling due to coupling to a heat bath; and (iii) generation of heat, limited by activation, from the reactants. The second effect, Newtonian cooling, describes the simplest manner in which we can incorporate the effect of a background heat bath fixed at a temperature significantly lower than the rest of the reaction area.[6] While this provides a sensible and physically motivated method of coupling reaction and diffusion to a thermal bath, it should be noted that it may be worthwhile to investigate other stabilizing mechanisms. The amount of heat generated in an activated process depends on the type of combustion system, or more generally reaction–diffusion system, one is examining. We describe the evolution of the temperature field by

$$\frac{\partial T}{\partial t} = D\,\nabla^2 T - \Gamma[T - T_0] - \mathbf{V}\cdot\nabla T + R(T, C) \tag{1}$$

where $D$ is the thermal diffusion coefficient, $\Gamma$ is the thermal dissipation constant, and $T_0$ is the constant background temperature of the bath to which the combustion process gives up heat through Newtonian cooling. The term $R(T, C)$ is responsible for chemical activation. For completeness we have included convection due to an external source $\mathbf{V}$, but we shall hereafter set this term to zero.

Nonlinearities enter through the reaction rate $R(T, C)$, which is limited by the local concentration of reactants $C(\mathbf{x}, t)$, where $C(\mathbf{x}, t)$ represents the local reactant fraction. The specific form of $R(\mathrm{C}, T)$ is dependent on the type of combustion process in question. Empirically, heat production in any combustion process is give by the exothermic reaction

$$R(T, C) \propto T^{\alpha} e^{-A/T} C \tag{2}$$

[6] Newtonian cooling implies heat can be removed without diffusion. This stabilizes the constant-velocity motion of the flame. If, instead, only diffusion was present, we expect a flat front to be unstable by the Mullins–Sekerka mechanism.

where[3] $\alpha = \mathcal{O}(1)$ and $A$ is the activation energy for combustion (Boltzmann' constant has been set to unity). As the exponential in Eq. (2) must be of order one, the scale of the heat production is set by the activation energy, as $A^{\alpha}$. Similarly, the time constant in front of the proportionality sign will dictate the time scale of the burning process. It should be noted that while the precise form of $\alpha$ in Eq. (2) sets the energy scale in the problem, the main dynamics of burning is controlled only by the Arrhenius form $e^{-A/T}$.[7]

Here we use $\alpha = 3/2$. This can be motivated by a simple model where reactants burn in steady state with an ideal gas, and chemical by-products are ignored. The net effect of the reaction is to heat the air surrounding the reactant, elevating it to the (steady-state) temperature of combustion. The flux of molecules striking the reacting surface is $N_s = n(T/8\pi m)^{1/2}$, where $n$ is the number density of air, and $m$ is the mass per molecule of air. Since combustion is an activated process, the probability of a molecule reacting is proportional to $e^{-A/T}$ where, again, $A$ is the activation energy of the reaction. Thus the total number of molecules reacting is $N_r = N_s e^{-A/T}$. Since the combustion process occurs in a steady state with the surrouning air, the energy flux from the reactant is limited by the local energy flux of air molecules striking it, given by $3T/2$ per molecule. Hence the energy $Q$ released per unit reactant area and per unit time is given by $Q = (3T/2)\, N_s e^{-A/T}$. Denoting the typical area by $a_t$ and the typical volume by $v_t$, the total energy produced per unit volume and per unit time in a region of local reactant concentration $C(\mathbf{x}, t)$ is given by $P_C = (Qa_t/v_t)\, C$. For a cylindrical reactant geometry where the height is much greater than the radius, $a_t/v_t = 2/r$. We then write

$$P_C = (3n/2r)(2/\pi m)^{1/2}\, q(T)\, C \tag{3}$$

where

$$q(T) = T^{3/2} e^{-A/T} \tag{4}$$

Thus the local energy produced per unit time and volume is proportional to $q(T)$, where the additional factor $T^{3/2}$ sets the scale of the energy, we model the reaction rate in Eq. (1) as

$$R = \lambda_2 q(T)\, C = -\lambda_1 \frac{\partial C}{\partial t} \tag{5}$$

[7] Simpler models without an Arrhenius form, where the reaction is given by a polynomial, are also of interest in the combustion literature. It should be noted that some of the results from those investigations have wider applicability than might otherwise be expected. See ref. 17 and references therein. The larger issue of the simplest model of combustion necessary to describe some phenomena, in essence the question of universality classes for combustion, is an important one which merits further study.

where $\lambda_1$ is a dimensionless constant. The constant $\lambda_2$ is simply the prefactor of $P_C$ divided by $c_p\rho$ and multiplied by $A^{3/2}$, where $c_p$ is the specific heat and $\rho$ is the mass density of air. This gives us the dimensionless temperature change per unit time corresponding to the heat production $P_C$. This completes the formulation, which thereby gives a rough estimate of the parameters involved in our model.

The main emphasis in the present work will be for cases where the initial distribution of the concentration field $C(\mathbf{x}, t=0)$ is random, and where no complete analytic solutions of Eqs. (1)–(5) are available.

For the remainder of this, we consider a two-dimensional geometry, where a front initially parallel to the $y$ axis propagates in the $x$ direction. The dimensionless parameters are set to $D=0.2$, $\Gamma=0.05$, $T_0=0.01$, and $\lambda_1=8$, and time is measured in units of those for the reaction, $\lambda_1/\lambda_2$, and length in units of the dimension in the reactant. In our numerical work, we initially distribute the reactant randomly such that at a given latice site $C(\mathbf{x}, t)=1$ with probability $c$ and zero with probability $1-c$, in which case the average spatial concentration of reactants is $c$. The mesh size in space is set to $\Delta x=1$, while the mesh size in time is $\Delta t=0.01$; tests of smaller mesh sizes give qualitatively similar results. It is useful to relate these choices of parameters to the specific example of a forest fire. For example, the constant $\Delta_2$ can be found in terms of the density and specific heat of air and the activation temperature of wood. In physical units, we have $D\sim 1\ \mathrm{m^2\,s^{-1}}$, $\Gamma\sim 0.05\ \mathrm{s^{-1}}$, $T_0\sim 0.1\ \mathrm{K}$, and $c_p\sim 5\ \mathrm{J\,g^{-1}\,K^{-1}}$ and $A\sim 500\ \mathrm{K}$. With the exception of $T_0$, these are comparable to real systems. Our small $T_0$ has been chosen to give enchanced cooling and hence keep diffusion fields relatively short ranged as compared to the lattice sizes used. This allows us to perform our numerical integrations with good accuracy without having to simulate extremely large systems. Test runs show that our results are relatively insensitive to the choice of $T_0$, as one would expect provided $T_0$ is much less than the reaction energy heat released $A$.

## 3. DYNAMICS OF FRONT PROPAGATION

### 3.1. Qualitative Features of Flame Fronts

Before presenting a quantitative analysis of Eqs. (1) and (5), it is useful to qualitatively examine the nature of their solutions. Due to the activated nature of the combustion process, we expect that a self-sustaining propagating combustion front requires a sufficient amount of heat to be released during combustion. The source for this heat is dependent on the reactant concentration $c$. Since activation limits the production of heat, we expect the existence of a critical concentration $c^*>0$ below which the fire

will spontaneously burn out due to insufficient heat production. That is, for $c < c^*$ the average velocity of the front is zero, while it is nonzero for higher concentrations. For $c > c^*$ the reaction front can be identified by a single-valued function which will be used in all quantitative analysis. We define the local position of the interface $h(y, t)$ as the position $x$ where the temperature field is maximum at a given time and coordinate $y$. The variable $h(y, t)$ is a single-valued function of $y$. Thus, the average velocity of the interface is given by $v(c) = \langle \partial h(y, T)/\partial t \rangle$.

(a)

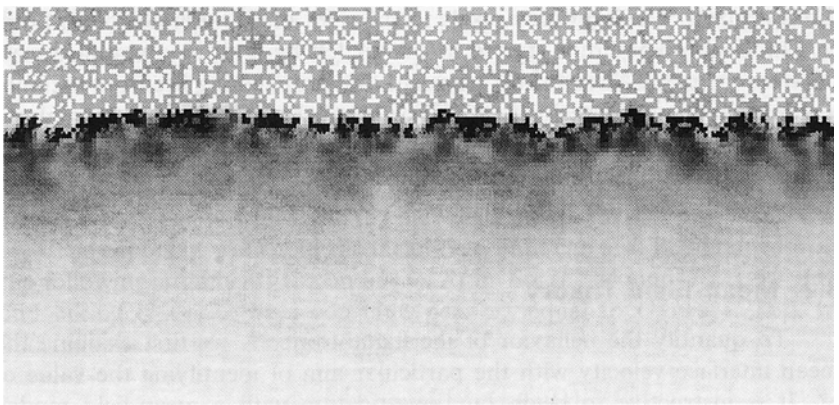

(b)

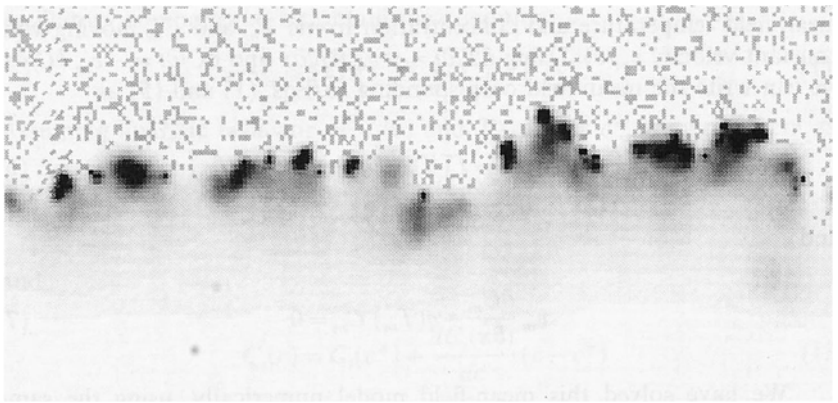

Fig. 1. The temperature field $T(x, y, t)$ for a moving fire front in a uniform, random forest with (a) $c = 0.65$ and (b) $c = 0.225$. The dark pixels correspond to the temperature field; the higher the temperature, the darker the pixels. The interface $h(x, t)$ is defined by the curve outlined by the darkest pixels. The light grey pixels above the interface represent reactant (trees).

In Figs. 1a and 1b typical configurations of the propagating temperature field are shown for $c = 0.65$ and 0.225. Equations (1) and (5) were solved on a lattice using periodic boundary conditions in the $y$ direction and fixed boundary conditions in the $x$ direction. The size of the system is $L$ in the $y$ direction, while in the $x$ direction it well exceeds the total diffusion length of the propagating $T$ field. The $T$ field is always contained within the system size due to a tracking program that continuously follows the flame front, which is moving toward the right. The dark pixels correspond to the temperature field, with the highest temperature corresponding to the darker pixels. The interface $h(x, t)$ is outlined by the darkest pixels. The light grey pixels to the right of the interface correspond to $C(\mathbf{x}, 0) = 1$. The fire is started at the far left by igniting a complete row of "trees" at $y = 0$. After a short transient, the propagating fire front assumes a steady-state average velocity $v(c)$. For lower densities approaching about 0.2, the front becomes very irregular and finally stops propagating. This is in agreement with our qualitative arguments; below we will present a quantitative analysis of this phenomenon.

### 3.2. Mean-Field Theory

To quantify the behavior of the flame front $c^*$, we first examine the mean interface velocity with the particular aim of identifying the value of $c^*$. It is instructive to begin our investigation with a mean-field model. Consider a uniform distribution of reactants whose initial density variable $C(\mathbf{x}, 0)$ at every site is now equal to a constant $c$. In this description there are no longer variations in $T$ or $C$ in the y direction. Assume there exist mean-field temperature and concentration fronts $T_m$ and $C_m$ moving with constant velocity $v_m(c)$. Using $\partial T/\partial t = -v_m\, \partial T/\partial x$ and $\partial C/\partial t = -v_m\, \partial C/\partial x$, we can write the mean-field corresponding to Eqs. (1) and (5) as

$$D\frac{\partial^2 T_m}{\partial x^2} + v_m \frac{\partial T_m}{\partial x} - \Gamma[T - T_0] + \lambda_1 C_m q(T_m) = 0 \tag{6}$$

and

$$v_m \frac{\partial C_m}{\partial x} - q(T_m)\, C_m = 0 \tag{7}$$

We have solved this mean-field model numerically, using the same procedure as described in Section 3.1, with $C(\mathbf{x}, 0) = c$. We solved for the mean-field front velocity, obtaining a dependence of $v_m(c)$ on $c$ of the form $v_m(c) \propto (c - c^*)^{\phi}$ near $c^* = 0.19$, where $\phi = 0.5$.

The existence of a finite critical concentration $c^*$ can also be seen by examining Eq. (6). Integrating Eq. (6) from $-\infty$ to $+\infty$, we obtain

$$\int_{-\infty}^{\infty} [\lambda_1 C_m q(T_m) - \Gamma(T_m - T_0)]\, dx = 0 \tag{8}$$

Equation (8) tells us that in order to have a steady state, the energy produced by activation must balance that lost due to thermal dissipation. There are two points where the integrand of Eq. (8) is identically zero. The first $x_h$ lies behind $\max(T_m)$, while the second $x_f$ lies ahead of it. This point $x = x_f$ can thus be defined via

$$\lambda_1 C_m(x_f)\, q(T_m(x_f)) = \Gamma(T_m(x_f) - T_0) \tag{9}$$

where for values of $c^*$ we have found that $C_m(x_f) \approx c$. Inspection of Eq. (9) shows that $T_m(x_f)$ increases as $C_m(x_f) \approx c$ decreases. Moreover, $\max(T_m)$ clearly decreases as $c$ decreases. Thus, since $T_m(x_f) \leqslant \max(T_m)$ there must exist a $c = c^*$ below which Eq. (8) no longer holds.

The exponent $\phi = 1/2$ in the mean-field limit can also be obtained from the following argument. Expanding $q(T)$ in Eq. (6) around $T_f(c) \equiv T_m(x_f)$ and taking $C_m(x)$ to be a constant, near $x_f$, equal to $C_f(c) \equiv C_m(x_f)$, we find that the leading edge of $T_m$ goes as

$$T_m \sim \exp\left( - \frac{v_m + \{v_m^2 - 4D[\lambda_1 C_f q'(T_f) - \Gamma]\}^{1/2}}{2D} x \right) \tag{10}$$

By imposing the requirement that the leading edge does not develop any oscillatory components, we obtain the condition

$$v_m \geqslant \{4D[\lambda_1 C_f q'(T_f) - \Gamma]\}^{1/2} \tag{11}$$

Assuming analytic behavior of $C_f(c)$ and $T_f(c)$ near $c^*$, we write them as

$$T_f(c) = T_f(c^*) + \frac{dT_f(c^*)}{dc}(c - c^*) \tag{12}$$

and

$$C_f(c) = C_f(c^*) + \frac{dC_f(c^*)}{dc}(c - c^*) \tag{13}$$

In regions ahead of the temperature field where thermal dissipation exceeds thermal activation ($x \geqslant x_f$), we have already noted that the concentration profile $C_m$ will not change from its original value $c$. Thus, around $x = x_f$ we

can approximate $C_t(c) \approx c$. Using this approximation in Eq. (13), which along with Eq. (12) is substituted into Eq. (11), we obtain

$$v_m \geqslant A(c - c^*)^{1/2} \tag{14}$$

which yields $\phi = 1/2$ and implicitly defines $c^*$ through $c^* = \Gamma/[\lambda_1 q'(T_t(c^*))]$. The constant

$$A = \left\{ 4D\lambda_1 \left[ q'(T_t(c^*)) + c^* q''(T_t(c^*)) \frac{dT_t(c^*)}{dc} \right] \right\}^{1/2} \tag{15}$$

Although we could have expanded the $q(T)$ term of Eq. (6) about any point, choosing $x_t$ gives the maximum lower bound in Eq. (11). This result is also supported numerically. This analysis leading to Eq. (14) is analogous to that used in ref. 5 to find front velocities in the context of epidemic models. Near $c^*$ we expect $v(c)$ to attain its lower bound,[5] according to Eq. (14).

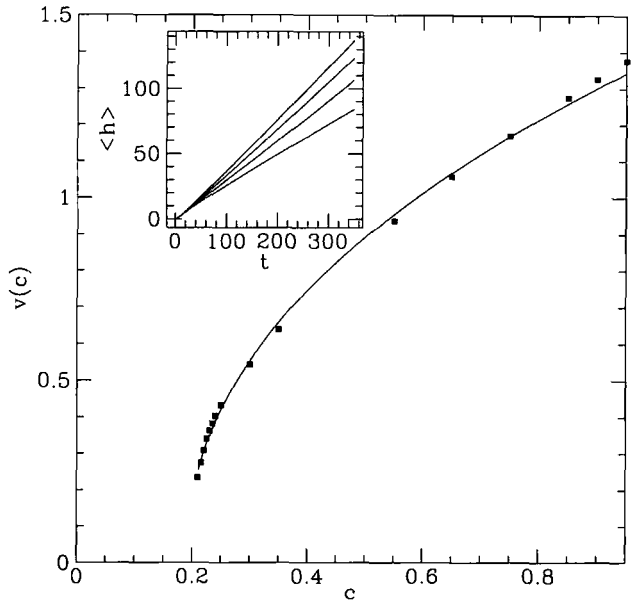


Fig. 2. Scaling of the interface velocity to the form $v(c) \sim (c - c^*)^{\phi}$ in the case of a random initial reactant distribution. This curve was fit using concentrations up to $c = 0.85$ and $L = 200$. The inset shows data of $\langle h \rangle$ vs. $t$ for $c = 0.21$, 0.22, 0.23, 0.24.

### 3.3. Numerical Results for Front Propagation

Equations (1) and (5) were numerically solved on a lattice under the conditions described above, with a uniform random distribution of density with $\langle C(\mathbf{x}, t=0)\rangle = c$. We found that for large concentrations, the mean interface velocity $v(c)$ is again constant after an initial transient, and increases with $c$. The transient increases as $c^*$ is approached. As in the mean-field case, we expect that the vicinity of $c^*$, the asymptotic velocity is defined by the relationship $v(c) \sim (c - c^*)^{\phi}$, where $\phi$ is a scaling exponent. Specifically, the numerical determination $v(c)$ in the case of a random background gave $c^* = 0.19 \pm 0.02$ and $\phi = 0.46 \pm 0.09$ for a system $L = 200$. The scaling of $v(c)$ in the case of a random initial distribution of reactants is shown in Fig. 2.

To incorporate finite-size effects in a systematic fashion, we use the scaling form

$$v(c, L) \sim L^{-\phi/\nu} \Omega[(c - c^*) L^{1/\nu}] \tag{16}$$

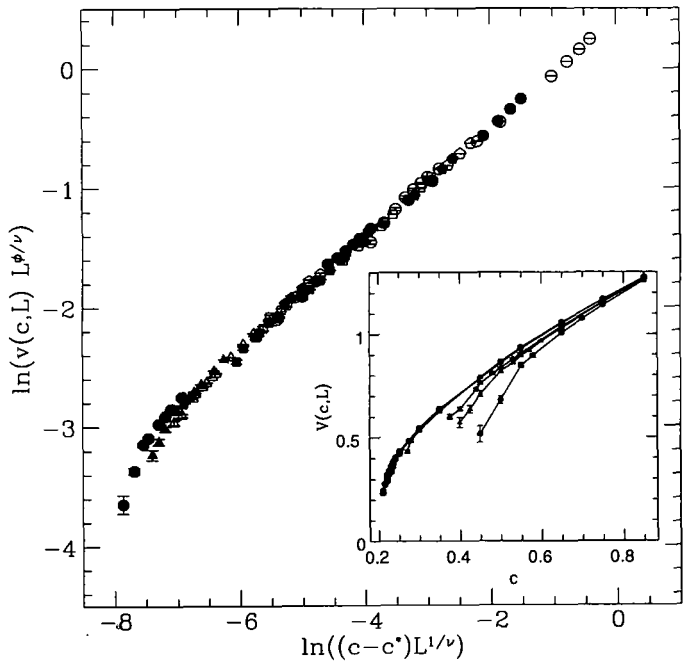


Fig. 3. Finite-size scaling of $v(c, L)$. The main figure shows $\ln[v(c, L) L^{\phi/\nu}]$ vs. $\ln[(c - c^*) L^{1/\nu}]$. The inset shows the unscaled data for system sizes $L = 4$, 6, 8, 24, 44, 54, 64, 104, and 200 from right to left. Sizes larger than $L = 24$ lie almost on the same curve. All systems contain data for $c$ up to and including $c = 0.85$.

This is the same as that used in percolation theory.[18] Here $\nu$ is the correlation length exponent $\xi \sim (c - c^*)^{-\nu}$, and the scaling function $\Omega(x \to \infty) \sim x^{\phi}$. We note that we can relate $\phi$ to the percolation transition exponents through $v(c) \sim \xi/\tau \sim (c - c^*)^{\Delta - \nu} \equiv (c - c^*)^{\phi}$, where $\Delta$ is the critical slowing down exponent. In Fig. 3, we show numerical results for $\ln[v(c, L)\, L^{\phi/\nu}]$ vs. $\ln[(c - c^*)\, L^{1/\nu}]$ for nine different system sizes ranging from $L = 4$ to $L = 200$. Using $c^* = 0.19$ and $\phi = 0.46$, we find that the best collapse occurs for $\nu = 0.6 \pm 0.1$.

It is striking that the results for the critical exponents obtained here are consistent with the mean-field theory of percolation, for which $\Delta = 2\phi = 2\nu = 1$.[19] Qualitatively, heat propagation in our model is limited by a percolation lattice, provided by the random density field $c$. Below $c^*$ the connected cluster available for front propagation breaks down, and the fire spontaneously dies out. The mean-field nature of the critical exponents is due to the relatively long range nature of the diffusion field associated with $T$ as compared to the typical front widths for the system sizes studied here.

## 4. KINETIC ROUGHENING OF THE FLAME FRONT

### 4.1. Numerical Results for the Front Roughening

For $c > c^*$ it is clear from Fig. 1 that the propagating interface associated with $T$ develops large fluctuations and appears rough. We can characterize the interface by defining its width through $w = \langle (h - \langle h \rangle) \rangle^{1/2}$. Rough interfaces often satisfy the scaling relation[15, 20]

$$w(t, L) \sim t^{\beta} f\left(\frac{t}{L^z}\right) \tag{17}$$

for large $L$ and $t$, where $f(x \to \infty) = x^{-\chi/z}$ and $f(x \to 0) \sim \text{const}$ with $\chi = z\beta$. An important example of this is the Kardar–Parisi–Zhang (KPZ) interface equation,[15] for which the exact and nontrivial exponents are $\beta = 1/3$, $z = 3/2$, and $\chi = 1/2$, for a one-dimensional interface (growth front). In our case, for any given value of $c > c^*$ we expect the width to obey the scaling form, i.e., for large $t$ we expect $w \sim t^{\beta}$ in the limit $t \ll L^z$. We similarly expect that when $t \gg L^z$ the width will scale with the system size via $w \sim L^{\chi}$.

These scaling forms for the interfacial width can be derived from a more general crossover scaling scaling ansatz that couples time, system size, and concentration. Near $c = c^*$ this scaling form is written as

$$w(c, t, L) = \xi(c)\; W\left(\frac{t}{\tau(c)}, \frac{L}{\xi(c)}\right) \tag{18}$$

where $W(x, y) \to w_s(x)$ for $x/y^{\zeta} \ll 1$, with $x_s(x) \sim x^{\beta}$ for $1 \ll x \ll y^{\zeta}$, and $W(x, y) \to w_L(y)$ for $x/y^{\zeta} \gg 1$, with $w_L(y) \sim y^{\chi}$ for $y \to \infty$. Near the percolation threshold $\tau(c) \sim (c - c^*)^{-\Delta}$ and $\xi \sim (c - c^*)^{-\nu}$. With these forms of $\tau(c)$ and $\xi(c)$, the scaling function in Eq. (18) couples $t$, $c$, and $L$ analogously to the way in which $t$, $c$, and cluster mass are coupled when describing transport on percolation clusters.[21]

In the limit $t \ll [\tau(c)/\xi^{\zeta}(c)]\, L^{\zeta}$ Eq. (18) reduces to

$$w(c, t) = \xi(c)\, w_s\left(\frac{t}{\tau(c)}\right) \tag{19}$$

where as $x \gg 1$, $x_s(x) \sim x^{\beta}$, leading to $w(t) \sim t^{\beta}$. In Fig. 4 we show the scaled width $w_s$ plotted vs. the scaled time $t_s = t/\tau$ for seven different values of $c$ with $L = 200$. For this $L$, finite-size effects seem to play no discernible role. The inset shows the original data set. A transient time $t_0$ has been subtracted, which has been determined from the point where $v(c)$ reaches

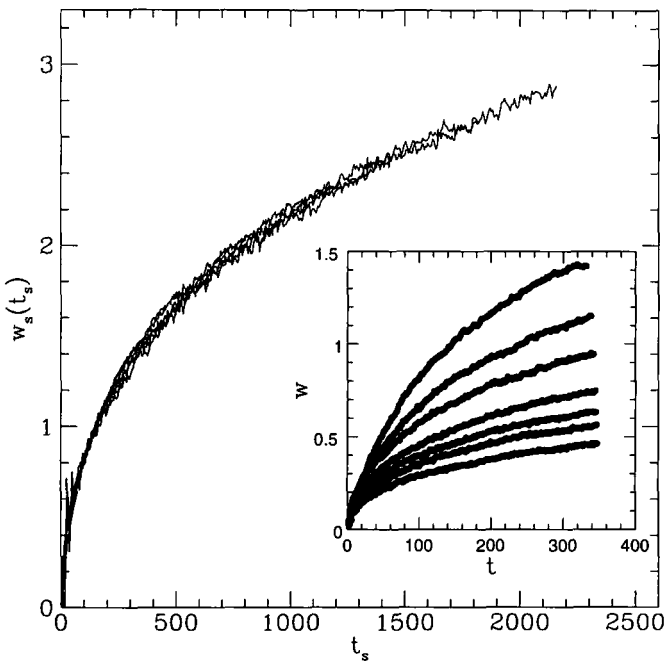


Fig. 4. Crossover scaling function $w_s$ plotted vs. $t_s = t/\tau$. The inset shows the concentration-dependent width $w(c, t)$ for $c = 0.4$, 0.5, 0.6, 0.7, 0.75, 0.80, and 0.85 from top to bottom. The roughness increases with decreasing density. A transient time $t_0$ and the corresponding offset $w_0$ have been subtracted from each $w(c, t)$.

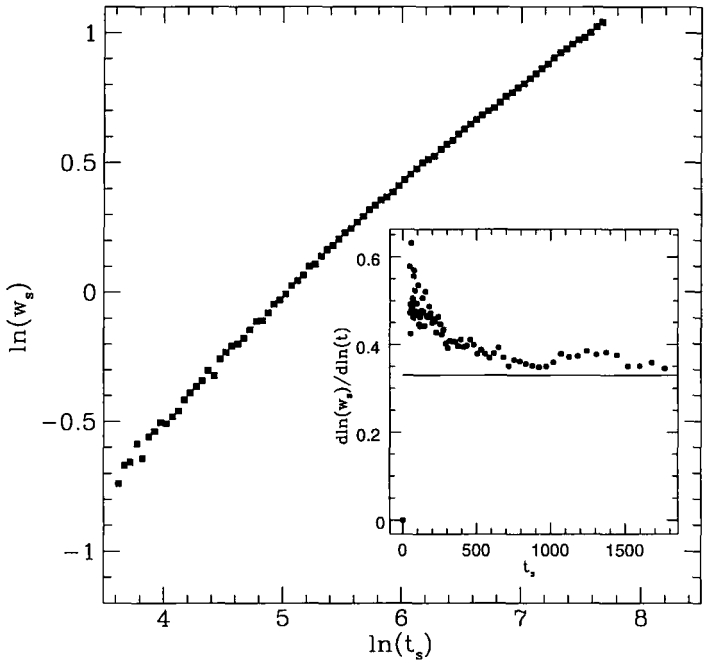


Fig. 5. A log–log plot of the scaling function $w_s$ of Fig. 4. The inset shows the effective $\beta$ as a function of time. The straight line represents $\beta = 1/3$.

a constant value. From the fitted $\xi(c)$ and $\tau(c)$ for the data collapse we cannot accurately estimate $\nu$ and $\Delta$, although they are again consistent with the mean-field values.

From the scaled data of Fig. 4 we can determine the roughening exponent $\beta$. The running slope of the data from a log $w_s$ vs. log $t_s$ gives an effective exponent $\beta(t)$, which is shown in Fig. 5. After an initial transient the slope clearly tends toward $\beta = 1/3$, which is the exact KPZ value. We have also analyzed the data by calculating the difference $w(bt) - w(t) = A(b^\beta - 1)\, t^\beta$, were $b$ is a constant (e.g., $b = 2$). From this method we find $\beta = 0.34 \pm 0.04$, which is our best estimate for the exponent.

When $t \gg [\tau(c)/\xi^z(c)]\, L^z$ Eq. (18) reduces to

$$w(c, L) = \xi(c)\, w_L\left(\frac{L}{\xi(c)}\right) \tag{20}$$

In this limit the width saturates due to finite-size effects and thus Eq. (20) is independent of time. In the limit of large $L$ the saturated width satisfies

$$w(c, L) \sim L^\chi \tag{21}$$

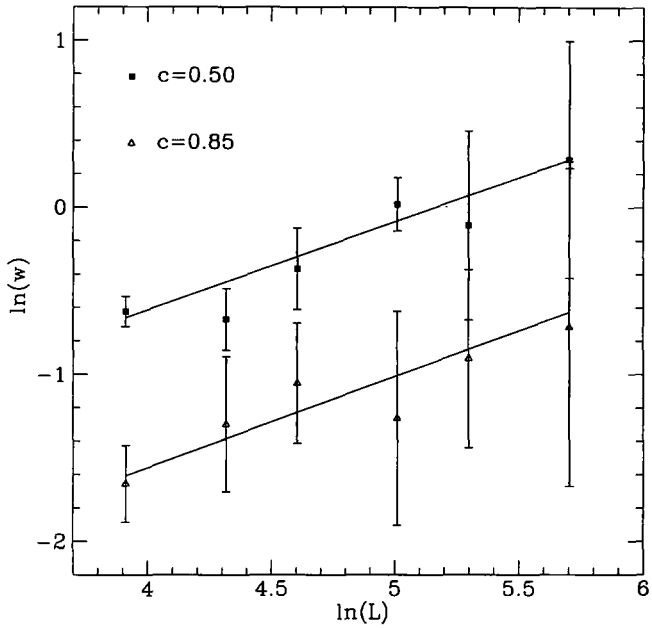


Fig. 6. Plots of $\ln(w)$ vs. $\ln(L)$ for $c=0.5$ and 0.85. The slopes give, respectively, $\chi=0.5\pm0.1$ and $\chi=0.5\pm0.3$, both consistent with the exact KPZ value of $\chi=1/2$.

Using system sizes $L=50$, 76, 100, 150, 200, 300, 400, and 600, we obtain $\chi=0.5\pm0.1$ for $c=0.5$ and $\chi=0.5\pm0.3$ for $c=0.85$. The plots yielding these values of $\chi$ are shown in Fig. 6. In both cases the value of $\chi$ is consistent with the exact KPZ value of $\chi=1/2$. Our results for $\beta$ and $\chi$ are therefore in good agreement with those of the KPZ equation.[15], [8]

We also note that a plausible way of expressing the crossover scaling function, for large $L$ and $t$, is in the form

$$w(t, c, L) \sim (c-c^*)^{\Delta\beta-\nu}\, t^{\beta} F\left(\frac{t}{(c-c^*)^{z\nu-\Delta}\, L^z}\right) \tag{22}$$

where $F(x\to\infty)\to x^{-\chi/z}$ and $F(x\to 0)\to$ const, with $z=\chi/\beta$. Equation (22) gives explicitly the $c$-dependent generalization of the scaling form of Eq. (17). We have not, however, been able to test this particular ansatz with our present data.

[8] Recently Zhang *et al.*[22] have interpreted the results of burning sheets of paper in terms of kinetic roughening. They found $\chi\sim 0.71$, which is larger than we find. This may be due to the correlated distribution of fibers within paper.

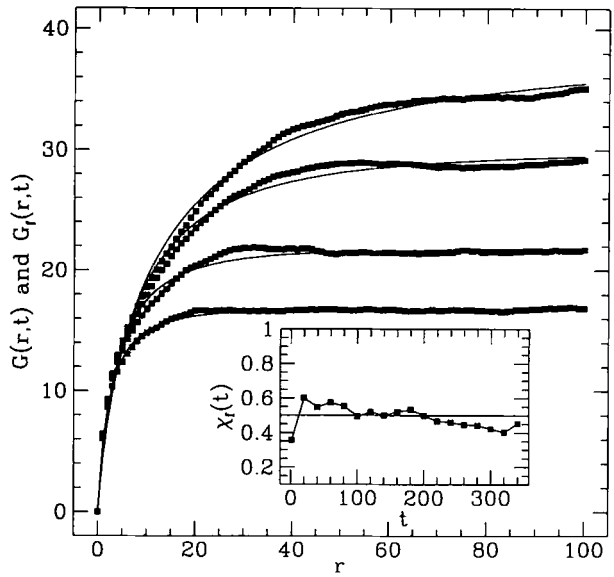


Fig. 7. Correlation function $G(r, t)$ and the fitted function $G_f(r, t)$ (solid line) versus $r$ at different times for $c = 0.5$. The higher curves represent larger times. The fitting function is given in the text. The inset shows $\chi_f(t)$ versus time with the straight line representing the exact KPZ value of $\chi = 1/2$.

Another quantity that can be used to characterize kinetic roughening is the equal-time height difference correlation function, which is defined by

$$G(r, t) = \langle [h(y + r, t) - h(y, t)]^2 \rangle \tag{23}$$

Asymptotically $G(r, t)$ satisfies

$$G(r, t) \to r^{2\chi} \tag{24}$$

for $r \ll t^{1/z}$, while for $r \gg t^{1/z}$ (with $t$ fixed)

$$G(r, t) \to G(t) \sim t^{2\beta} \tag{25}$$

While these limits can in principle be used to extract $\chi$ and $\beta$, determining the asymptotic limits poses practical problems. They have been overcome, however, by developing a functional fitting ansatz for $G(r, t)$.[23] This ansatz can be used to fit the whole function $G(r, t)$ and allows the extraction of estimates for all the scaling exponents $\beta$, $\chi$, and $z$. We have adapted this method by using the fitting form

$$G_f(r, t) = A(t)\{\tanh[B(t)^{1/x} r^{2\chi_f(t)/x}]\}^x \tag{26}$$

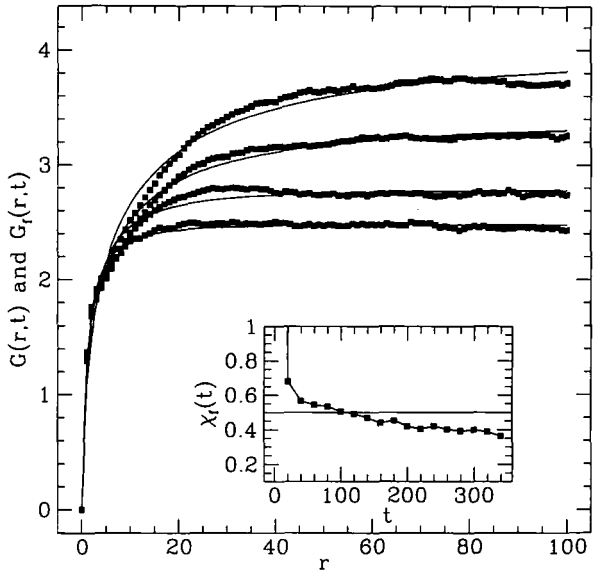


Fig. 8. Correlation function $G(r, t)$ and the fitted function $G_f(r, t)$ (solid line) versus $r$ for $c = 0.85$. See text for details.

where $A(t)$, $B(t)$, and $\chi_f(t)$ are fitting parameters, while $x$ is fixed. In the limit $1 \ll L^z \ll t$, $G_f(r, t) = A(t)\, B(T)\, r^{2\chi_f(t)}$, which allows the estimation of $\chi \approx \chi_f(t)$, as discussed below. In the other limit of $r \gg t^{1/z}$, $G_f(r, t) \to A(t) \sim t^{2\beta}$. We have not tried the latter estimate here, however.

In Fig. 7 the correlation function is plotted at various times for $c = 0.5$. The data are fit to the form of Eq. (26). The value of $x$ is first determined from fitting $G(r, t)$ at one particular time, and is subsequently held fixed for all other times. For $c = 0.05$, $x = 3$ gives the best results. The inset of Fig. 7 shows $\chi_f(t)$, with the solid line representing the exact KPZ value of $\chi = 1/2$. After a short initial transient, $\chi_f(t)$ becomes roughly a constant and is consistent with the KPZ value. In Fig. 8 the correlation data for $c = 0.85$ are shown. For $c = 0.85$ we found that $x = 4$ fits the data most accurately for all times. From the inset of Fig. 8, we see that $\chi_f(t)$ is again consistent with 1/2.

## 4.2. Derivation of the Front Equation

For $c$ near unity, it is possible to derive analytically an approximate equation of motion describing the flame front of our model of Eqs. (1)–(5).

We can imagine the temperature field as being composed of the steady-state mean-field $T_m$ plus a small perturbation $\delta T$ caused by nonuniformities in the reactant distribution. This approximation becomes more accurate as $C(\mathbf{x}, 0)$ approaches a uniform distribution. Also, as we take the system size to infinity, we can systematically average out local fluctuations along the interface and retain an equation governing the long-wavelength dynamics of the interface.

We first introduce a relative coordinate system by the transformation $x = X(u, s)$ and $y = Y(u, s)$, where $u(x, y) = \text{const}$ are a set of planes parallel to the interface, while $s$ is the arclength along the constant-$u$ plane. Defining $u_t(s, t) = \partial u/\partial t$, we write the equations for $T$ and $C$ in these coordinates as

$$\frac{\partial T}{\partial t} + u_t \frac{\partial T}{\partial u} = D \nabla^2_{s,u} T - \Gamma[T - T_0] + \lambda_1 q(T)\, C \tag{27}$$

$$u_t \frac{\partial C}{\partial u} = -q(T)\, C \tag{28}$$

where the $\nabla^2_{u,s}$ operator in Eq. (27) is given by

$$\nabla^2_{u,s} = \frac{\partial^2}{\partial u^2} + K(s) \frac{\partial}{\partial u} + \frac{\partial^2}{\partial s^2} \tag{29}$$

and $K(s)$ is the curvature.[9] In Eq. (28) we assume that the reactant field changes much faster than the thermal field, thus dropping the $\partial C/\partial t$ term. This is quite common in reaction–diffusion systems.[26]

Solving first Eq. (28), we obtain

$$C = \eta(s, t) \exp\left( \int_u^{\infty} \frac{q(T(z, s, t))}{u_t(s, t)}\, dz \right) \tag{30}$$

where $\eta(s, t)$ comes from the boundary conditions, which demand that $C(\infty, s, t)$ be either zero or one, with the same distribution as the original $C$ field. Statistically, $\eta(s, t)$ is a Bernoulli random variable with $\langle \eta \rangle = c$. The boundary condition as $u \to -\infty$ is that $C$ vanishes. This is satisfied since $u_t = -v$, where $v$ is the normal velocity.

Next we examine $T$ equation. We represent the $T$ field as $T = T_m(u) + \delta T(u, s, t)$, where $T_m$ is the mean-field solution. Substituting this expression for $T$ and the form of $C$ given by Eq. (30) into Eq. (27), we obtain, to first order in $\delta T$,

[9] See, e.g., refs. 24. A clear description of this technique is given by Rogers.[25]

$$u_t \frac{\partial T_m}{\partial u} = D \frac{\partial^2 T_m}{\partial u^2} + DK(s) \frac{\partial T_m}{\partial u} - \Gamma[T_m - T_0] + \lambda_1 \eta(s, t)\, S(T_m(u), u_t) + P \cdot \delta T + \lambda_1 \eta(s, t) \times S(T_m(u), u_t) \left( I[\delta T] + \frac{q'(T_m)\, \delta T}{q(T_m)} \right) \tag{31}$$

where the operator $P$ is given by

$$P = \nabla^2_{s,u} - \frac{\partial}{\partial t} - u_t \frac{\partial}{\partial u} - \Gamma \tag{32}$$

and the function $S(T_m(u), u_t)$ is defined by

$$S(T_m(u), u_t) = q(T_m(u)) \exp\left( \int_u^\infty \frac{q(T_m(z, s, t)}{u_t(s, t)}\, dz \right) \tag{33}$$

with

$$I[\delta T] = \int_u^\infty \frac{q'(T_m(z))}{u_t} \delta T(z, s, t)\, dz \tag{34}$$

Next we multiply Eq. (31) by $\partial T_m/\partial x$ and integrate the resulting equation over $(-\varepsilon, \infty)$, where $\varepsilon$ is defined as a point to the left of $\max(T_m)$. In performing this integration, we are essentially following the methods for deriving interface equations.[24,25] For such a method, the "projecting field" $T_m$ must assume two states over the range $(-\varepsilon, \infty)$. A simple calculation shows that the trailing edge of $T_m$ [defined on $x < \max(T_m)$] goes as $T_m \sim \exp(-\Gamma |x|/v)$, while we can write the leading edge [defined on $x > \max(T_m)$] as $T_m \sim \exp(-v\,|x|/D)$. For our $\Gamma$, the field $T_m$ can be approximated by a constant for a certain distance, $\varepsilon$ to the left of $\max(T_m)$. Conversely, since $v/D \gg \Gamma$, the leading edge of $T_m$ falls to $T_0$ much faster than the trailing edge. Thus, over the range for which the reaction front is defined, we can treat $T_m$ as a two-state function. Performing the projection onto $T_m$, we arrive at

$$\frac{\partial u}{\partial t} = DK(s) - \frac{\Gamma \Lambda}{\sigma} + \frac{\lambda_1 \eta(s, t)}{\sigma} \times \int_{-\varepsilon}^\infty \frac{dT_m}{du} S(T_m(u), u_t)\, du + \frac{1}{\sigma} \int_{-\varepsilon}^\infty \frac{dT_m}{du} \left\{ P \cdot \delta T + \lambda_1 \eta(s, t)\, S(T_m(u), u_t) \left[ I[\delta T] + \frac{q'(T_m)}{q(T_m)} \delta T \right] \right\} du \tag{35}$$

where the constants $\sigma$ and $\Lambda$ are defined by

$$\sigma = \int_{-\varepsilon}^{\infty} \left( \frac{dT_m}{du} \right)^2 du \tag{36}$$

and

$$\Lambda = \int_{-\varepsilon}^{\infty} \frac{dT_m}{du} [T_m(u) - T_0] \, du \tag{37}$$

Since we are interested in the equation of motion of the reaction front as the system $L \to \infty$ and as the wavenumber $k \to 0$, we integrate out the effect of the short wavelengths by introducing the operator

$$\Omega(f(u, s', t)) = \langle f(u, s', t) \rangle_{(s - L_B/2 < s' < s + L_B/2)} \tag{38}$$

where $L_B$ represents the distance over which the function $f(u, s', t)$ is averaged. This operator smooths over a distance $L_B$ along the interface, thus eliminating wavenumbers larger than $2\pi/L_B$. We now proceed to rewrite Eq. (35) with respect to $s'$ and apply $\Omega$ to both sides of the equation.

The first four terms in Eq. (35) are simplified by expressing $u_t$ as

$$u_t(s', t) = u_t(s, t) + \delta v(s', t) \tag{39}$$

where $u_t(s, t)$ is the normal velocity obtained after averaging over the block $s - L_B/2 < \dot{s} + L_B/2$. Applying $\Omega$ to $u_t(s', t)$ and treating $\delta v(s', t)$ as a random variable with zero mean, we arrive at $\Omega(u_t(s', t)) = u_t(s, t)$. In a similar manner the curvature and the constant term in Eq. (35) are just rewritten in terms of $s$ when operated on by $\Omega$. Using Eq. (39) and expanding $S(T_m(u), u_t)$, the integrand in the fourth term in Eq. (35) gives

$$\frac{\lambda_1}{\sigma} \eta(s', t) \, S(T_m(u), u_t(s, t)) \left[ 1 - \frac{\delta v(s', t)}{u_t(s, t)} \int_u^{\infty} \frac{q(T_m(z))}{u_t(s, t)} dz \right] \tag{40}$$

Now, it is reasonable to assume that the fluctuating variables $\eta(s', t)$ and $\delta v(s', t)$ are statistically independent with $\delta v(s', t)$ having zero mean in the limit where $L_B \to \infty$. Thus, applying $\Omega$, the fourth term in Eq. (35) becomes

$$\frac{\lambda_1}{\sigma} \hat{\eta}(s, t) \int_{-\varepsilon}^{\infty} \frac{dT_m(u)}{du} S(T_m(u), u_t(s, t)) \, du \tag{41}$$

where $\hat{\eta}$ is the noise under the action of $\Omega$. Assuming, further, that $\delta T$ and $\delta v(s', t)$ are also uncorrelated with $\delta T$ having zero mean, we can similarly

show that the fifth term involving $\delta T$ goes to zero under the action of $\Omega$. Thus, after smoothing over $L_B$ where $L_B \to \infty$, the equation of motion for the reaction front becomes

$$\frac{\partial u}{\partial t} = DK(s) - \frac{\Gamma \Lambda}{\sigma} + \frac{\lambda_1}{\sigma} \hat{\eta}(s, t) \int_{-\varepsilon}^{\infty} \frac{dT_m}{du} S(T_m(u), u_t)\, du \tag{42}$$

To simplify Eq. (42), we note that the time derivative of the interface $\partial h/\partial t$ is given by

$$\partial h/\partial t = [1 + (\partial h/\partial x)^2]^{1/2} v \tag{43}$$

where $v = -\partial u/\partial t$ is the normal velocity to the interface. Also we write the curvature in terms of the function $h(x, t)$ as

$$K = -[1 + (\partial h/\partial x)^2]^{-3/2} \partial^2 h/\partial x^2 \tag{44}$$

Furthermore, let us approximate $u_t$ in the function $S(T_m(u), u_t)$ appearing in Eq. (42) by $u_t \approx -v_m$, where $v_m$ is the (as yet undetermined) mean interface velocity. Finally we note that we can write the noise term $\hat{\eta}$ as $\hat{\eta} = \hat{\mu} + c$, where $c$ is the average reactant density and $\langle \hat{\mu} \rangle = 0$. Using the definitions of this last paragraph in Eq. (42) and writing $h(x, t) = v_m t + \hat{\zeta}(x, t)$, we obtain, after expanding to second order in derivatives of $h(x, t)$;

$$\frac{\partial \hat{\zeta}}{\partial t} = D \frac{\partial^2 \hat{\zeta}}{\partial x^2} + \frac{1}{2\sigma} (\Gamma \Lambda + \hat{\lambda}_1 c) \left( \frac{\partial \hat{\zeta}}{\partial x} \right)^2 + \frac{\hat{\lambda}_1}{\sigma} \hat{\mu} \tag{45}$$

where we identify $v_m = \Gamma \Lambda/\sigma + \hat{\lambda}_1 c/\sigma$, and $\hat{\lambda}_1$ is given by

$$\hat{\lambda}_1 = -\lambda_1 \int_{-\varepsilon}^{\infty} \frac{dT_m(u)}{du} S(T_m(u), -v_m)\, du \tag{46}$$

The noise term at the interface, $\hat{\mu}$, is a Bernoulli-distributed random variable, which by the central limit theorem becomes normally distributed as $L_B \to \infty$. Thus, the equation of motion we have derived for the flame front is equivalent to the KPZ equation of interfacial roughening in the long-wavelength limit.

## 5. SUMMARY AND DISCUSSION

In this work we have developed a realistic phase-field model for the dynamics of slow combustion in a randomly distributed medium. Our model is derived from the first principles of chemical kinetics, assuming a

reactant burns via a steady-state reaction with air. In addition to chemical activation, our model also includes thermal diffusion and thermal dissipation. An important property of our model is the existence of a continuously extended thermal field, through the diffusive coupling of the thermal field to the concentration field of the reactant. We define the parameters of our model based on the properties of wood, and motivate our combustion problem in the context of forest fires.

We find a percolation transition at a critical density $c^* \approx 0.19$, below which the flame front will spontaneously die. We have analyzed the nature of this transition showing that the velocity of the average front position scales as $(c-c^*)^{\phi}$, where $\phi \approx 1/2$. We also found a correlation exponent $\nu \approx 1/2$. Both these values are consistent with the mean-field theory of percolation as well as the mean-field limit of combustion we derived from the full equations. Through analyzing our mean-field model, the existence of a critical concentration is also found analytically.

Above $c^*$ we found that the interface associated with the combustion front displays kinetic roughening. By an appropriate application of the scaling theories developed for percolation theory and kinetic roughening of interfaces, we have derived a scaling ansatz for the interfacial width that couples time, concentration, and system size. This form has been verified numerically in appropriate limits, and used to estimate the scaling exponents $\beta$ and $\chi$ independently. Together with the equal-time height–height correlation function, the results give strong evidence to the fact that the kinetic roughening of the flame front is in the universality class of the KPZ equation. We have also obtained this result analytically, by deriving an approximate interface equation which, near $c=1$, is equivalent to the KPZ equation.

While our model was derived to describe combustion fronts, it also lends itself to the description of a wider class of activated reaction–diffusion problems. Provided the reaction term contains an Arrhenius factor, the prefactor $T^{\alpha}$ multiplying the activated form plays a less important role in determining the properties of the equation. Thus, we belive that a wide class of different physical systems, described by equations analogous to Eq. (1), show behavior of the type described here. Of course, one of the main ingredients in the present work has been the introduction of a *random* background density field of reactants, which leads to the kinetic roughening of the front.

## ACKNOWLEDGMENTS

The Centre for Scientific Computing (CSC) of Espoo, Finland, has provided most of the computing resources for this work. This work has

also been supported by the Academy of Finland, the Natural Sciences and Engineering Research Council of Canada, and the Fonds pour la Formation de Chercheurs et l'Aide à la Recherche de Québec.

## REFERENCES

1. J. Krug and H. Spohn, In *Solids Far from Equilibrium: Growth, Morpology, and Defects*, G. Godreche, ed. (Cambridge University Press, Cambridge, 1991).
2. R. Kapral, *J. Math. Chem.* **6**:113 (1991).
3. F. A. Williams, *Combustion Theory*, 2nd ed. (Benjamin Cummings, 1985).
4. M. N. Chee, S. G. Whittington, and R. Kapral, *Physica D* **32**:438 (1988).
5. J. D. Murray, *Mathematical Biology*, (Springer-Verlag, Berlin, 1989).
6. R. Kapral, R. Livi, G.-L. Oppo, and A. Politi, *Phys. Rev. E* **43**:3 (1994).
7. J. C. Roux, R. H. Simoyi, and H. L. Swinney, *Physica D* **8**:257 (1983).
8. G. I. Sivashinsky, *Acta Astronaut.* **4**:1177 (1977).
9. M. L. Frankel and G. I. Sivashinsky, *Combust. Sci. Technol.* **29**:207 (1982).
10. G. Albinet, G. Searby, and D. Stauffer, *J. Phys.* **47** (Paris):1 (1986); G. Mackay and N. Jan, *J. Phys. A* **17**:L757 (1984).
11. P. Bak, K. Chen, and C. Tang, *Phys. Lett. A* **147**:297 (1990).
12. B. Drossel and F. Schwabl, *Phys. Rev. Lett.* **69**:1629 (1992); P. Grassberger and H. Kantz, *J. Stat. Phys.* **63**:685 (1991).
13. L. D. Landau and E. M. Lifshitz, *Fluid Dynamics* (Pergamon Press, Oxford, 1959), Chapter XIV.
14. N. Provatas, T. Ala-Nissila, M. Grant, K. R. Elder, and Luc Piché, *Phys. Rev. E* (1994), in press.
15. M. Kardar, G. Parisi, and Y. C. Zhang, *Phys. Rev. Lett.* **56**:889 (1986).
16. P. Bak, C. Tang, and K. Wiesenfeld, *Phys. Rev. Lett.* **59**:381 (1987).
17. A. P. Aldushin, S. I. Khudyaev, and Y. B. Zel'dovich, *Archivum Combustionis* **1**:9 (1981)
18. D. Stauffer and A. Aharony, *Introduction to Percolation Theory*, 2nd ed. (London, Taylor and Francis, 1992).
19. D. Stauffer, *Phys. Rep.* **54**:3 (1979).
20. F. Family and T. Vicsek, *J. Phys. A* **18**:L75 (1985).
21. R. B. Pandey, D. Stauffer, A. Margolina, and J. G. Zabolitzky, *J. Stat. Phys.* **34**:427 (1984).
22. J. Zhang, Y. C. Zhang, P. Alström, and M. T. Levinsen, *Physica A* **189**:383 (1992).
23. T. Ala-Nissila, T. Thjelt, and J. M. Kosterlitz, *Europhys. Lett.* **19**(1):1 (1992); T. Ala-Nissila, T. Hjelt, J. M. Kosterlitz, and O. Venäläinen, *J. Stat. Phys.* **72**:207 (1993); T. Ala-Nissila and O. Venäläinen, *J. Stat. Phys.* (1994), to appear.
24. B. Grossmann, H. Guo, and M. Grant, *Phys. Rev. A***43**:1727 (1991); K. R. Elder, J. Viñals, and M. Grant, *Phys. Rev. A* **46**:7618 (1992)
25. T. M. Rogers, Ph.D. thesis, University of Toronto, unpublished (1989).
26. A. K. Kapila, In *Asymptonic Treatment of Chemically Reacting Systems*, A. Jeffrey, ed. (Pitman, Boston, 1983)